# HUBBLE SPACE TELESCOPE PROPER MOTION (HSTPROMO) CATALOGS OF GALACTIC GLOBULAR CLUSTERS. III. DYNAMICAL DISTANCES AND MASS-TO-LIGHT RATIOS[*]

Laura L. Watkins, Roeland P. van der Marel, Andrea Bellini, and Jay Anderson
Space Telescope Science Institute, 3700 San Martin Drive, Baltimore, MD 21218, USA; lwatkins@stsci.edu

## ABSTRACT

We present dynamical distance estimates for 15 Galactic globular clusters (GCs) and use these to check the consistency of dynamical and photometric distance estimates. For most of the clusters, this is the first dynamical distance estimate ever determined. We extract proper-motion (PM) dispersion profiles using cleaned samples of bright stars from the *Hubble Space Telescope* PM catalogs recently presented in Bellini et al. and compile a set of line of sight (LOS) velocity-dispersion profiles from a variety of literature sources. Distances are then estimated by fitting spherical, non-rotating, isotropic, constant mass-to-light ratio (*M/L*) dynamical models to the PM and LOS dispersion profiles together. We compare our dynamical distance estimates with literature photometric estimates from the Harris GC catalog and find that the mean fractional difference between the two types is consistent with zero at just $-1.9 \pm 1.7\%$. This indicates that there are no significant biases in either estimation method and provides an important validation of the stellar-evolution theory that underlies photometric distance estimates. The analysis also estimates dynamical *M/L*s for our clusters; on average, the dynamically inferred *M/L*s agree with existing stellar-population-based *M/L*s that assume a Chabrier initial mass function (IMF) to within $-8.8 \pm 6.4\%$, implying that such an IMF is consistent with our data. Our results are also consistent with a Kroupa IMF, but strongly rule out a Salpeter IMF. We detect no correlation between our *M/L* offsets from literature values and our distance offsets from literature values, strongly indicating that our methods are reliable and our results are robust.

*Key words:* globular clusters: general – globular clusters: individual – proper motions – stars: distances – stars: kinematics and dynamics – stars: luminosity function, mass function

*Supporting material:* machine-readable tables

## 1. INTRODUCTION

Globular clusters (GCs) are among the first objects to have formed in the universe, within 1 Gyr of the Big Bang. They are some of the oldest objects for which ages are known and, thus, provide crucial constraints on the age of the universe itself (e.g., Vandenberg et al. 1996; Carretta et al. 2000; Krauss & Chaboyer 2003). As Verde et al. (2013) pointed out, local measurements of cosmological parameters (such as the age of the universe) are valuable, as they provide cosmology-independent tests of favored cosmological models.

Three primary methods are used to estimate GC ages: luminosity of the main-sequence turnoff (MSTO, e.g., Chaboyer 1995); white-dwarf (WD) cooling curves (Hansen et al. 2002); and nucleocosmochronology (radioactive age dating of stars, e.g., Cowan et al. 2002). The MSTO luminosity method is the most common, however, it requires an accurate determination of the observed magnitude of the MSTO, accurate reddenings, and accurate distances. Advances in photometric instrumentation have provided both the depth and precision necessary to pinpoint the MSTO within cluster CMDs. Reddening maps, such as those presented in Schlafly & Finkbeiner (2011), fulfill the second requirement. However, cluster distances are still poorly determined and distance uncertainties dominate over other sources of error in age determinations. There are two key points we need to address: (1) we must ensure that we are measuring distances accurately; (2) we must ensure that different distance measures agree (i.e., our methods are not biased).

Cluster distances are also useful to obtain for their own merit. They constitute an important rung on the short end of the distance ladder, which can again have implications for the verification of cosmological models. Furthermore, distances provide a third dimension of positional phase space. Many clusters are coincident with substructures in the Galactic halo (e.g., Bellazzini et al. 2003; Mackey & Gilmore 2004; Martin et al. 2004); distances to the clusters (and to the substructures) can help us determine if there is simply a chance alignment of cluster and substructure along the line of sight (LOS) or if they are truly associated. Evidence of tidal tails has also been found around some clusters (e.g., Niederste-Ostholt et al. 2010; Küpper et al. 2015) and other clusters have been posited as progenitors for tidal streams of undetermined origin; distance information can help in both cases by providing extra information with which to constrain cluster orbits. Cluster orbits, in turn, can help to constrain the shape of the inner Galactic halo.

Cluster distances can be estimated from both photometric and kinematic data. Photometric studies typically estimate distances via the distance modulus, defined as the difference between the apparent and absolute magnitudes of a given object or population. Apparent magnitudes are relatively easy to obtain. Absolute magnitudes are only well defined for certain types of objects, often called "standard candles." Periodic variables, such as Cepheids and RR Lyraes, are common standard candles in the local universe, although even their absolute magnitudes depend on the metallicity of the star and the period of their variability (e.g., Catelan et al. 2004). Nevertheless, they are very useful distance indicators and are widely used; not only for cluster-distance estimation (e.g., Del Principe et al. 2006), but also for many other science

---

applications, including to identify substructure in and trace the shape of the Galactic halo (e.g., Watkins et al. 2009).

Kinematic studies estimate distances by comparing LOS velocity dispersions and proper-motion (PM) velocity dispersions. These quantities are measured in different units; converting from one set of units to the other requires knowledge of the distance. Or, conversely, by assuming that the dispersions are equal (or different in some known and quantifiable way), the distance can be estimated. Very few kinematic distance estimates exist, as only very few clusters have measured internal PMs.

Although, kinematic and photometric distance estimates use very different data sets and very different methods, their estimates should, of course, be the same for any given cluster. Until now, it has been difficult to assess the agreement (or lack thereof) between kinematic and photometric distance estimates due to the scarcity of kinematic distance estimates. However, in the few cases where both photometric and kinematic estimates do exist, they often disagree (e.g., Del Principe et al. 2006; Watkins et al. 2013).

Pinpointing the source of the disagreement is complicated by the fact that both types of estimate are usually made on a cluster-by-cluster basis. So when comparing a set of photometric estimates with a set of kinematic estimates, it is difficult to determine whether any differences are due to systematic biases in either estimation method, or are due to scatter from study to study.

To make progress, we need large, homogeneous sets of distance estimates: larger samples will provide more robust statistics; homogeneity in the distance estimation process will eliminate some potential sources of disagreement so we can be confident we are making a meaningful comparison.

Most GC distances have been measured in individual studies, however, fortunately there is a large photometric distance analysis that suits our purposes: Harris (1996, 2010 edition, hereafter H96) provided a catalog of cluster properties (including distances) for 157 Galactic GCs. No large study has yet been done for dynamical distance estimates, as the kinematic data has simply not been available. We require both LOS and PM data; although both types of data are lacking, the dearth of PM data has, so far, been the limiting factor for kinematic distance estimates.

This situation has recently changed. In Bellini et al. (2014, hereafter Paper 1), we presented a set of *Hubble Space Telescope* (*HST*) PM catalogs for 22 GCs in the Milky Way. The catalogs were compiled following a search through archival *HST* data to find fields in Galactic GCs that had been previously observed at multiple epochs for different projects. The exquisite astrometric sensitivity of *HST*, coupled with baselines of up to 12 years (achievable thanks to the archival nature of the project), allowed us to measure PMs with exceptional precision. For typical clusters in our sample, the bright, well-measured stars have measurement uncertainties of just 32 $\mu$as yr$^{-1}$ ($\sim$1.2 km s$^{-1}$ at a distance of 8 kpc, which is typical for our clusters). Another advantage of these catalogs is the sheer volume of data they encompass: the median number of stars in the full catalogs is $\sim$60,000, and following certain selection cuts as we will describe in Section 2, we use a median of 3000 stars per cluster for the analysis we present here.

These catalogs were compiled with two key drivers: (1) to facilitate more-detailed studies of each individual cluster; and (2) for the insight we can gain by considering the population of

clusters as a whole. There is a wide range of science questions that can be addressed both for individual clusters and for the whole population, too many to consider in detail here, but see the introduction of Paper 1. Here, we seek to advance both goals.

In Watkins et al. (2015, hereafter Paper 2), we presented kinematical profiles and maps for the bright stars in each of the 22 clusters. Here we build on this analysis by comparing our kinematics with previous LOS studies in order to estimate distances for the clusters. This is the first dynamical distance study performed for more than a handful of clusters, and greatly increases the number of dynamical distances available for Galactic GCs. By comparing these dynamical distances estimates with photometric estimates from the literature, we can assess the consistency of photometric and kinematic distance-estimation methods.

Section 2 introduces the PM catalogs, LOS literature data and surface brightness profiles we use for our study. In Section 3, we briefly outline our distance estimation method and, in Section 4, we use it to estimate distances for our clusters. In Section 5, we provide context for our results via comparison with previous studies, and look at statistics for the sample as a whole. We conclude in Section 6.

## 2. CLUSTER DATA

To estimate cluster distances, we require both PM and LOS velocity-dispersion profiles. For our analysis, we use the *HST* PM catalogs described in Paper 1, to which we refer for detailed explanations of the data reduction and processing. We augment these catalogs with LOS velocity data available in the literature. Although Paper 1 provides catalogs for 22 Galactic GCs, here we are only able to use the clusters for which LOS dispersion profiles have been published or for which LOS velocity catalogs have been published containing sufficient stars from which to determine a dispersion profile. Of the 17 clusters with both PM and LOS data, we exclude NGC 6362 and NGC 7099 (M30), as our PM data sets are too small (following the cuts we make below) for our distance estimation procedure.

As we will see in Section 3, we also require a Multi-Gaussian-Expansion (MGE)[1] fit to the surface brightness profile for each cluster. Fortunately surface brightness profiles are available for all of our clusters so we do not need to further cut our sample. This leaves us with 15 clusters in total for this study.

Here we briefly describe the PM catalogs, the literature LOS data, the surface brightness profiles we use, and the MGE fitting process.

### 2.1. Proper-motion Catalogs

GCs are collisional systems; as the stars undergo a series of two-body interactions, they exchange energy and slowly move toward a state of energy equipartition. As a result, low-mass (faint) stars tend to move faster than high-mass (bright) stars. Recently, Trenti & van der Marel (2013) showed that clusters never reach full equipartition, but nevertheless, even in partial equipartition, we still expect that stars of different mass will exhibit different kinematic properties. Thus, to estimate distances via the comparison of PM and LOS dispersion

---

[1] MGEs are examples of finite mixture models (McLachlan & Peel 2000).

profiles, we must ensure that both measurements are for stars of similar masses. LOS studies are typically limited only to the brightest stars; most data is collected from ground-based facilities and only spectra of bright stars achieve sufficient signal-to-noise to measure a velocity. As such, we must impose a magnitude cut on our PM sample to select stars of similar masses to those observed in LOS studies.

Furthermore, unbiased kinematics can only be extracted using stars for which positions (and hence PMs) have been accurately measured and for which uncertainties have been correctly estimated. Poor position measurements—particularly a problem in crowded fields where stars suffer greatly from blending—and underestimated error bars will both tend to artificially inflate the velocity distributions. The catalogs also contain some contaminants, both from the Milky Way and from other nearby objects, which must be removed.

In Paper 2, we described a series of cuts that we make to the PM catalogs to ensure that we have a reliable, high-quality sample of stars. We refer to Paper 2 for a detailed discussion of the cuts, but briefly outline the main points here.

1. Remove all stars fainter than 1 mag below the MSTO.
2. Remove all stars with $N_{used}/N_{found} < 0.8$, where $N_{used}$ is the number of data points used for the final calculation of the PM and $N_{found}$ is the total number of data points found for each star.
3. Remove all stars with $F_D\left(D\chi^2_{reduced}\right) > 0.99$, where the $\chi^2_{reduced}$ values are for the straight-line fits used to determine PMs, $F_D$ is the cumulative distribution function for a $\chi^2$ distribution with $D$ degrees of freedom and, here, $D = N_{used} - 2$.
4. Remove stars for which the quality of the point-spread function (PSF) fit was determined to be low. Quality of the PSF fit varies with both magnitude and position within the cluster, and also depends on the distance and concentration of the cluster. As such, the details of this step varied from cluster to cluster.
5. $3\sigma$ clip in velocity and remove all stars with PM errors larger than half the local dispersion. This is an iterative process to ensure that only "good" stars (i.e., measurements with enough signal) are used to define the boundaries of the final PM and PM error cuts.

For Paper 2, we required a limited range of stellar masses across our sample so that we could neglect the effect of stellar mass on the kinematics. It is this that motivated the initial magnitude cut. A cut 1 mag below the MSTO was adequate for our purpose of calculating spatial kinematic profiles. However, if we are to calculate accurate distances via comparison to LOS data, we must be more restrictive and impose a brighter magnitude cut. So, we take the final samples from Paper 2, extracted via the cuts listed above, and make a further magnitude cut, retaining only stars brighter than the MSTO.[2]

---

[2] In principle, we can make this revised magnitude cut at the MSTO in step 1; however, this significantly reduces the number of stars in the sample. We then find it difficult to perform the last two stages of the cleaning process effectively due to the nature of the cleaning algorithm. The two-stage magnitude cut we describe in the text is more effective, as it limits the mass-range of the initial sample while retaining enough stars with which to perform the rest of the cleaning.

## 2.2. Proper-motion Kinematic Profiles

We determine kinematic profiles from our PM data by binning the cleaned samples in radius and then calculating the mean and dispersion of the velocity in each bin. Our PM profiles measure the average one-dimensional PM in the plane of the sky, which corresponds to an average over the radial and tangential PM components (this is rigorously defined in Section 2.6 of van der Marel & Anderson 2010).

When binning stars, we need to ensure that we have sufficient stars with which to calculate reliable dispersions, but we also want to maximize the spatial resolution of our bins. As the spatial coverage of the data is highly inhomogenous, we find that a variable binning scheme is best suited to our needs. Then the kinematics in each bin are determined using a maximum-likelihood estimation method that fully accounts for biases. Both the binning scheme and the maximum-likelihood kinematic estimation are described in full in Paper 2, to which we refer the reader for further details.

As described above, the final PM samples we use for this paper are different from those we used in Paper 2 as we performed an additional magnitude cut for our present study. As a result, the kinematic profiles are not the same as those used in Paper 2.

### 2.3. Line of Sight Velocity and Proper-motion Literature Data

Where possible, we use LOS velocity-dispersion profiles taken directly from previous studies. However, dispersion profiles are not always available; in that case, we use the published stellar catalog of LOS velocities and determine our own velocity-dispersion profile. To do this, we proceeded similarly as for our PM data: we binned the stars in radius (albeit with a simpler binning scheme[3]) and used the same maximum-likelihood method to determine the kinematics in each bin.

Four clusters also have published PM velocity-dispersion profiles; we will later show these profiles in comparison to our own but will not use them as part of our distance estimation. All sources of literature data are shown in Table 1; for each cluster we list the references for the source and the type of data taken from the source (LOS dispersion profiles, LOS stellar catalogs, or PM dispersion profiles).

We also show the compilations of literature data for each of our clusters in Figure 1. Cluster names are shown in the bottom-left corner of each panel. Points are colored according to source and data type (LOS or PM), as indicated in the legends; colors are different in each panel. Source references were abbreviated, the full references are given in Table 1. These compilations are also available in Appendix B.

### 2.4. MGE Fits to Surface-brightness Profiles

We begin with the Chebyshev polynomial fits to the $V$-band surface brightness profiles given in Trager et al. (1995). These are observed profiles and do not account for interstellar reddening. If we only cared about distances, we could proceed straight away with the uncorrected profiles, as we only need the shape of the luminosity profile for our subsequent analysis, not the normalization factor. However, as a by-product of our analysis, we will also be able to estimate cluster mass-to-light

---

[3] For the LOS data sets, we separated the stars into $N$ equally populated bins, where $N$ was chosen separately for each data set; we did not use the variable-binning algorithm used for our PM dispersion profiles.

**Table 1**
Sources for Literature Data

| Cluster (1) | Source (2) | Type (3) |
|---|---|---|
| NGC 104 | Gebhardt et al. (1995) | LC |
| | McLaughlin et al. (2006) | LD, PD |
| | Lane et al. (2010) | LD |
| NGC 288 | Scarpa et al. (2007) | LD |
| | Sollima et al. (2012) | LD |
| NGC 1851 | Scarpa et al. (2011) | LD |
| | Carretta et al. (2011) | LC |
| | Lützgendorf et al. (2013) | LD |
| | Lardo et al. (2015) | LD |
| | K. Larson & A. Seth (2015, private communication) | LD |
| NGC 2808 | Carretta et al. (2006) | LC |
| | Lützgendorf et al. (2012) | LD |
| | Lardo et al. (2015) | LD |
| | K. Larson & A. Seth (2015, private communication) | LD |
| NGC 5139 | van de Ven et al. (2006) | LD, PD |
| | Sollima et al. (2009) | LD |
| | van der Marel & Anderson (2010) | PD |
| | Noyola et al. (2010) | LD |
| | Scarpa & Falomo (2010) | LD |
| NGC 5904 | Kimmig et al. (2015) | LC |
| NGC 5927 | Lardo et al. (2015) | LD |
| | Simmerer et al. (2013) | LC |
| NGC 6266 | McNamara et al. (2012) | PD |
| | Lützgendorf et al. (2013) | LD |
| NGC 6341 | Drukier et al. (2007) | LC |
| | Mészáros et al. (2009) | LC |
| | Kamann et al. (2014) | LD |
| | Kimmig et al. (2015) | LC |
| NGC 6388 | Lützgendorf et al. (2011) | LD |
| | Lanzoni et al. (2013) | LD |
| | Lapenna et al. (2015) | LD |
| NGC 6397 | Meylan & Mayor (1991) | LD |
| | Gebhardt et al. (1995) | LC |
| | Lovisi et al. (2012) | LC |
| | Heyl et al. (2012) | PD |
| NGC 6656 | Lane et al. (2009) | LD |
| | Zloczewski et al. (2012) | LC |
| NGC 6715 | Bellazzini et al. (2008) | LD |
| | Ibata et al. (2009) | LD |
| | Carretta et al. (2010) | LC |
| NGC 6752 | Carretta et al. (2007) | LC |
| | Sollima et al. (2012) | LD |
| | Zloczewski et al. (2012) | LC |
| | Lardo et al. (2015) | LD |
| NGC 7078 | Drukier et al. (1998) | LD |
| | McNamara et al. (2003) | PD |
| | van den Bosch et al. (2006) | LD, PD |
| | den Brok et al. (2014) | LD |
| | Lardo et al. (2015) | LD |
| | Kimmig et al. (2015) | LD |

**Notes.** Columns: (1) cluster identification in the NGC catalog; (2) reference for literature data; (3) type of data taken from source (LD—LOS velocity-dispersion profile, LC—LOS velocity stellar catalog, PD—PM velocity-dispersion profile).

ratio (M/L) ratios and masses; for these M/L and mass estimates to be meaningful, we must ensure the surface brightness profiles have been properly corrected. To do this, we use extinction values $A_V$ from Schlafly & Finkbeiner (2011).[4]

Next, we convert the surface brightness values from mag arcsec$^{-2}$ to $L_\odot$ pc$^{-2}$ via

$$\Sigma = \frac{1}{c^2}10^{-0.4\left(\mu - M_{V,\odot} + 5\right)}, \qquad (1)$$

where we have used $\Sigma$ to denote the surface brightness in units of $L_\odot$ pc$^{-2}$ and $\mu$ to denote the surface brightness in units of mag arcsec$^{-2}$. $M_{V,\odot} = 4.83$ mag is the V-band absolute magnitude of the Sun and $c = \pi/648{,}000$ rad arcsec$^{-1}$ is the conversion factor from arcsec to radians.

Finally, to perform the MGE fitting, we use the routine described in Cappellari (2002).[5] We start the fitting procedure with 15-component fits, however many of the final fits contain fewer Gaussian components as the routine itself discards components that make a negligible contribution to the overall profile. As an example, Figure 2 shows the surface brightness MGE for NGC 2808, broken down into its constituent Gaussians. The colored lines show the individual Gaussian components and the black line shows the total MGE profile.

The V-band surface brightness profiles and our MGE fits are shown in Figure 3. Both sets of data points are taken from Trager et al. (1995): red points show the surface brightness data, blue points show their Chebyshev polynomial fits. Our MGE fits to the Chebyshev polynomials are shown as black lines.

## 3. DISTANCE ESTIMATION METHOD

Dynamical distance estimation relies on the fact that LOS velocities are measured as physical distance per unit time, while PMs are measured as angular distance per unit time. To convert physical distance to angular distance, or vice versa, we require the distance to the object. For an object with PM $\mu$ (in mas yr$^{-1}$), its transverse velocity $v$ (in km s$^{-1}$) is given by

$$v = DC\mu, \qquad (2)$$

where $D$ is the distance of the object (in kpc) and $C$ is a constant that takes care of the remaining unit conversions.[6] Dispersions $\sigma_v$ and $\sigma_\mu$ scale similarly. So, if we knew both $\sigma_\mu$ and $\sigma_v$, we could then infer the distance to the object by finding the factor by which the PM velocity dispersion profile must be scaled to best match the LOS velocity dispersion. Of course, this implicitly assumes that the object is isotropic so that, by definition, the PM and LOS dispersions are the same. If the object is anisotropic, then the PM dispersion will be some factor of the LOS dispersion, and this must be accounted for in the distance estimation. We showed in Paper 2 that the clusters in our sample are very close to isotropic, particularly at their centers, so we will assume that the clusters are isotropic over the range for which we have data.

So by comparing the dispersion profiles we obtain from our PM catalogs against LOS velocity dispersion profiles from the literature, we can estimate distances to our clusters. However, our PM dispersion profiles and the LOS dispersion profiles are not sampled at the same radii, and even worse, in some cases

---

[4] In fact, we pulled the extinction values from the NASA/IPAC Extragalactic Database.

[5] While this fitting approach follows the commonly accepted procedure in stellar dynamics (e.g., van de Ven et al. 2006; van den Bosch et al. 2008; Emsellem et al. 2011; Lützgendorf et al. 2012; Feldmeier et al. 2013; Seth et al. 2014), we note that statistical literature suggests that alternative implementations (such as maximum likelihood estimation with expectation maximization) may be worth exploring in the future.

[6] $C = 4.74047$ km yr kpc$^{-1}$ mas$^{-1}$ s$^{-1}$.
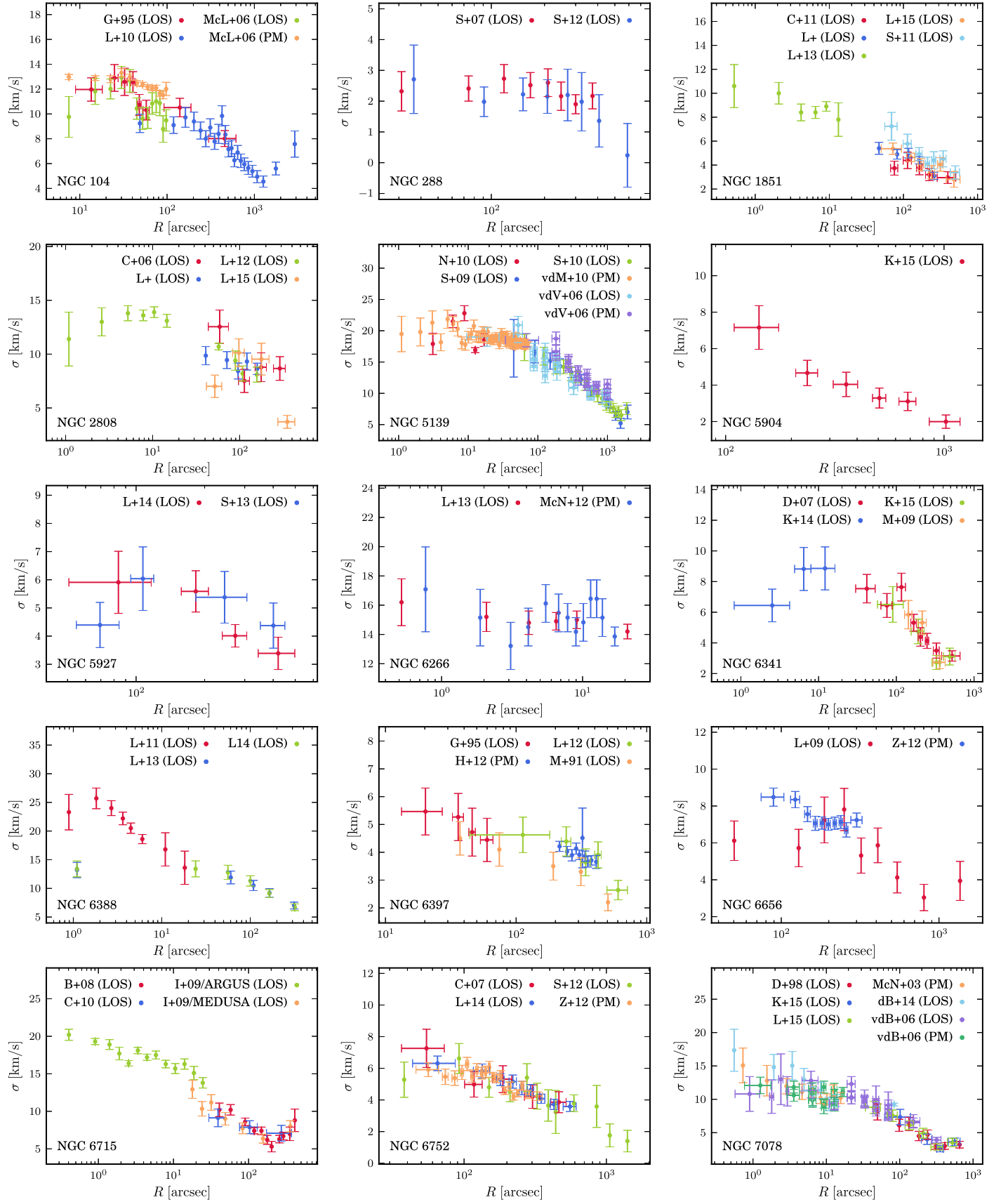
**Figure 1.** Compilations of literature dispersion profiles for each of our clusters. The cluster name is shown in the bottom left corner of each panel. The data sources and type of data (LOS or PM) are provided in the legend. The sources are abbreviated for convenience; for the full references see Table 1. PM data sets are shown at the distance provided in H96.
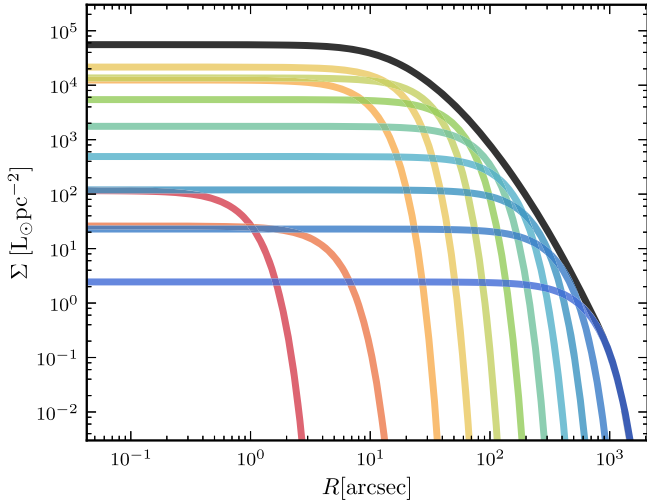
**Figure 2.** MGE fit to the surface-brightness profile for NGC 2808. The black line shows the full MGE profile and the colored lines show the individual Gaussian components.

the radial overlap is small or non-existent. This makes it challenging to determine for which distance the two profiles best agree. Therefore, instead of comparing profiles directly, we fit a simple dynamical model to both dispersion profiles and then determine for which distance the best-fit models agree. We determine the best-fitting models using maximum likelihood analysis.

Here we describe our dynamical models and then lay out the likelihood functions we use to assess the quality of the model fits.

### 3.1. Models

We use the Jeans Axisymmetric MGE (JAM) models described in Watkins et al. (2013), which were expanded from Cappellari (2008). We use only the model-predicted LOS dispersion profiles because under the assumption of isotropy the LOS and PM profiles are the same. The JAM models require projected luminosity-density and mass-density profiles, both in the form of an MGE. In general, these may be different; however, as we will discuss, we will assume that the mass-density profiles have the same shape as the luminosity-density profiles so that all that is required is the surface brightness profiles (already described in Section 2.4) and an M/L.

These models allow for axisymmetry, anisotropy, rotation and an M/L that varies with radius. However, for this study, we assume that the clusters are spherical, isotropic, non-rotating and have a constant M/L. These assumptions are typical of dynamical cluster studies (e.g., McLaughlin & Meylan 2003; Sollima & Nipoti 2010). Although typical, it does not necessarily follow that they are correct; however, in general, we believe that these assumptions are reasonable for most of the clusters. The exception is ω Centauri, which we know is highly flattened, shows significant rotation, and is anisotropic (e.g., van de Ven et al. 2006; van der Marel & Anderson 2010; Bianchini et al. 2013; Watkins et al. 2013) (although we do believe the M/L is constant (van de Ven et al. 2006)). Nevertheless, we include ω Centauri in our analysis; however, we will treat the results with caution. We will discuss the model assumptions in detail in Section 5.4.

### 3.2. Likelihood Functions

Let us assume that we have an LOS velocity-dispersion profile consisting of dispersions $\sigma_{L,i} \pm \delta_{L,i}$ (in km s$^{-1}$) measured at radii $R_{L,i}$ (in arcsec) and a PM velocity-dispersion profile consisting of dispersions $\sigma_{P,j} \pm \delta_{P,j}$ (in mas yr$^{-1}$) measured at radii $R_{P,j}$ (in arcsec). The units here are important, as we will see.

Let us also assume that we have a dynamical model for which we can calculate the dispersion $\sigma_{model}$ (in units of km s$^{-1}$) at radius $R$ for a given distance $D$ and M/L $\Upsilon$.[7] Under the assumptions we laid out above, both distance and M/L are the only free parameters in our models and both are multiplicative factors: the former because the models are typically calculated for $R$ in physical units whereas we require $R$ in angular units to compare with data; and the latter under the assumption that the M/L is constant through the cluster. In this case, the model dispersion is

$$\sigma_{model}(R, D, \Upsilon) = \sqrt{\frac{D\Upsilon}{D_0\Upsilon_0}}\,\sigma_{model}(R, D_0\Upsilon_0) \quad (3)$$

for some reference distance $D_0$ and M/L $\Upsilon_0$. This simplifies the modeling process, as we only need to calculate the model one time for $(D_0, \Upsilon_0)$ and can then scale the model appropriately.[8] For convenience, let us define

$$\sigma_0(R) = \frac{\sigma_{model}(R, D_0\Upsilon_0)}{\sqrt{D_0\Upsilon_0}}. \quad (4)$$

We use likelihood maximization to determine which models best fit the data. For a particular distance and M/L, the log-likelihood function for fits to the LOS velocity dispersion profile is

$$\ln \mathcal{L}_L(D, \Upsilon) = \sum_i - \frac{\left[\sqrt{D\Upsilon}\,\sigma_0(R_{L,i}) - \sigma_{L,i}\right]^2}{2\delta_{L,i}^2}. \quad (5)$$

With LOS velocities alone, the best we can do is determine the factor

$$f = \sqrt{D\Upsilon} \quad (6)$$

that is required to bring the model into good agreement with the data. We cannot distinguish how much of $f$ comes from the distance scaling and how much comes from the M/L scaling.

For the PM velocity dispersion profile, the log-likelihood function for a given distance and M/L is

$$\ln \mathcal{L}_P(D, \Upsilon) = \sum_j - \frac{\left[\frac{\sqrt{D\Upsilon}}{DC}b(R_{P,j})\sigma_0(R_{P,j}) - \sigma_{P,j}\right]^2}{2\delta_{P,j}^2}, \quad (7)$$

where the extra factor of $DC$ converts the units of $\sigma_0$ from km s$^{-1}$ to mas yr$^{-1}$ and $b(R)$ is an anisotropy term that controls the size of PM dispersions relative to the LOS dispersions. Under the assumption of isotropy, as we use here, $b = 1$ at all radii. Again, with PMs alone, the best we can do is determine

---

[7] As we use V-band surface brightness profiles in our dynamical models, all our M/Ls are in the V-band.

[8] In principle, we could use any reference values here; for simplicity, we will use reference distance $D_0 = 1$ kpc and reference M/L $\Upsilon = 1\,M_\odot/L_\odot$.
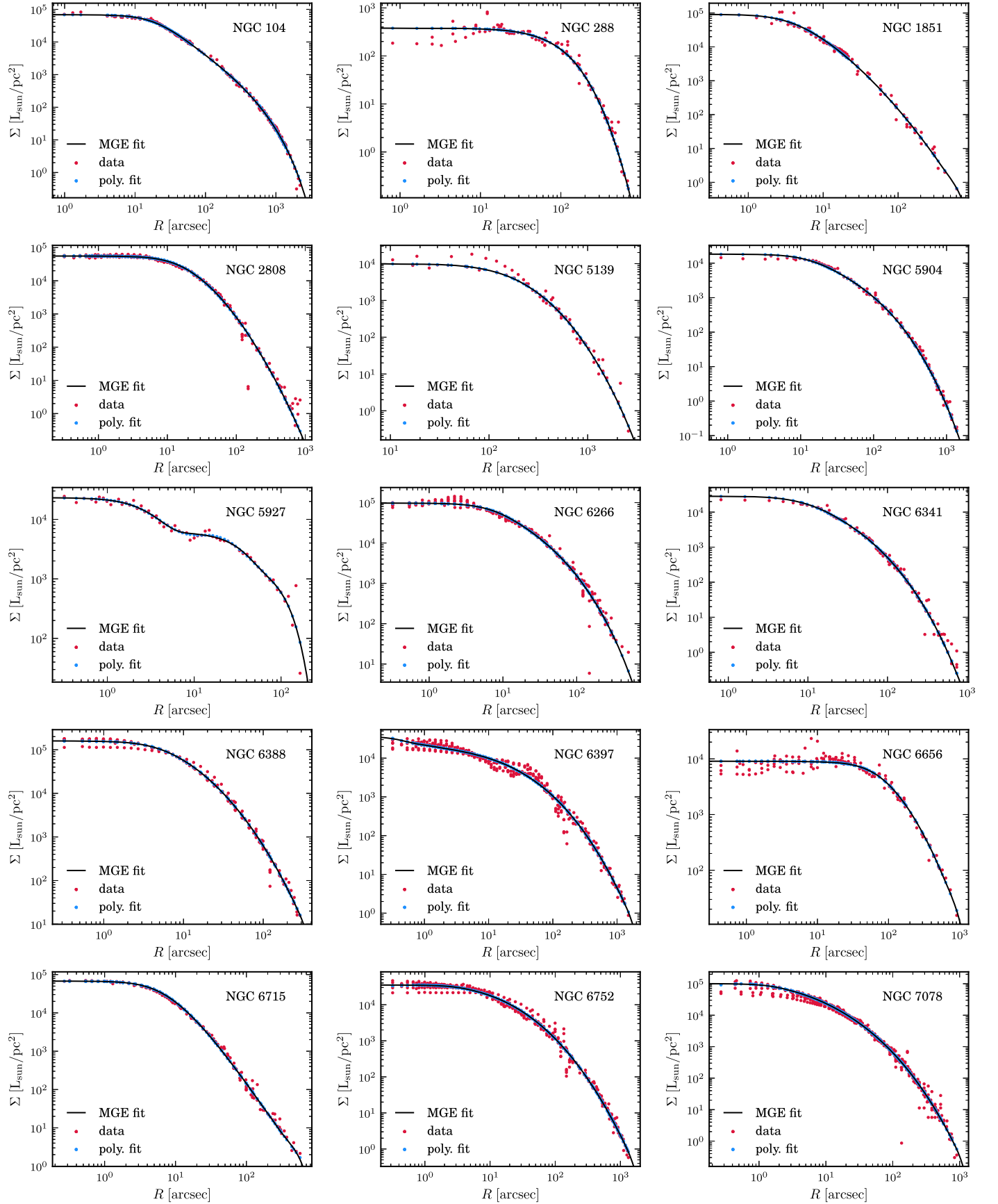
**Figure 3.** *V*-band surface brightness profiles for each cluster. The cluster name is shown in the top right corner of each panel. Red points shows the data compiled by Trager et al. (1995). Blue points show the Chebyshev polynomial fits from Trager et al. (1995). Black lines show our MGE fits to the Chebyshev polynomials.

the factor

$$g = \frac{\sqrt{D\Upsilon}}{D} = \sqrt{\frac{\Upsilon}{D}}, \qquad (8)$$

but we cannot distinguish the separate contributions made by distance and *M/L*.

However, with PMs and LOS velocities together, we can determine both distance *D* and *M/L* $\Upsilon$; the total log likelihood is then

$$\ln \mathcal{L}(D, \Upsilon) = \ln \mathcal{L}_{\mathrm{P}}(D, \Upsilon) + \ln \mathcal{L}_{\mathrm{L}}(D, \Upsilon). \qquad (9)$$

Although *D* and $\Upsilon$ are the free parameters of interest, they are highly correlated. As *f* and *g* are uncorrelated, they are more effective to use in a parameter search, as we illustrate in Section 4.1. So in practice, we seek to find factors *f* and *g*, then we determine distance *D* and *M/L* $\Upsilon$ via

$$D = \frac{f}{g} \qquad \text{and} \qquad \Upsilon = fg. \qquad (10)$$

## 4. RESULTS

Now that we have described both the data and the methods we will use, we are ready to estimate distances and *M/L*s for our clusters. Using the surface brightness profiles and *M/L* estimates, we can also estimate cluster masses.

### 4.1. Distance and Mass-to-light Ratio Estimates

To recap, we calculate spherical, isotropic, non-rotating JAM models for which we assume the *M/L* is constant. Under these assumptions, the model velocity-dispersion profiles have only two free parameters—distance *D* and *M/L* $\Upsilon$—and both are multiplicative factors. We fit these models to the literature LOS and our PM velocity dispersion profiles; by combining the two fits we can estimate the distance and *M/L* of the cluster.

To begin, we perform a simple likelihood maximization test using Equation (5) to approximate the best-fitting value of *f* and then a second simple likelihood maximization test using Equation (7) to approximate the best-fitting value of *g*. This gives us the region of parameter space where the best model is to be found, but does not give an indication of the scatter among the best-fitting models. To better sample the best-fit region, we then use the Markov Chain Monte Carlo (MCMC) package EMCEE developed by Foreman-Mackey et al. (2013), which is an implementation of the affine-invariant ensemble sampler by Goodman & Weare (2010); this approach uses multiple trial points (walkers) at each step to efficiently explore the parameter space. We run our MCMC chain with 100 walkers for 100 steps, and use the last 20 steps as the final sample.

To determine the distance and *M/L* for each cluster, we first use Equation (10) to convert the final MCMC sample from (*f*, *g*) space to (*D*, $\Upsilon$) space. Then we take the median values of each parameter as the best-fitting values and use the 15.9th and 84.1th percentile values as lower and upper uncertainty limits as these correspond to the 1$\sigma$ confidence interval.[9]

---

[9] These uncertainties reflect scatter in the parameter estimates due to random errors; they do not account for any additional sources of scatter that could arise if the modeling assumptions were relaxed. Note that we have not attempted to constrain the shape of the dispersion profile, we have simply used the model profile as a tool to help us match the LOS and PM data and estimate distances and *M/L* values. As such, the quoted uncertainties reflect the agreement between the LOS and PM data, not the goodness-of-fit of the model to the data.

As an example, Figure 4 shows the final parameter distributions at the end of the MCMC run for NGC 5927. The histograms show the distributions of the individual parameters with a best-fitting Gaussian shown as a black line. The scatter plots show the two-dimensional distributions of the parameters, with the points colored according to likelihood from high (red) to low (blue). The solid lines show the 50th percentiles the distributions and the dotted lines show the 15.9th and 84.1th percentiles of the distributions. The upper panels show the results for *f* and *g*, which show no correlation. The lower panels show the results for *D* and $\Upsilon$, highlighting their very strong correlation and illustrating why we run our MCMC chains in (*f*, *g*) space.

For five of our clusters—NGC 104, NGC 5139, NGC 5927, NGC 6388, and NGC 6715—we restrict the range of the literature LOS data used for the fitting to be only those data points that overlap with our PMs. As we discuss in detail in Appendix A, these cuts are an attempt to mitigate the effect of any inconsistencies outside of the range of our data.

In Figure 5, we show the results of our distance estimation; the cluster name is shown in the top right corner of each panel. The blue points show the literature LOS dispersion profiles used in the fitting process. The red points show our PM dispersion profiles, shifted to the best-fitting distance. The black lines show model profiles using 100 draws from the MCMC sampling. Our distance estimate, with uncertainties, is given in the bottom left corner of each panel. Where available, orange points show literature PM dispersion profiles shifted to the best-fitting distance; these are shown for comparison only and were not used for the fits. The best values of *f*, *g* and the corresponding distances and *M/L*s are given in Table 2; we also give the number of PM stars that survived the cleaning and magnitude cuts in Section 2 and were used for this analysis.

The model parameters we estimate here provide the best fit to the data under a particular set of assumptions, but this does not guarantee that the best-fitting model is actually a good fit to the data. A visual inspection of the model fits in Figure 5 can give an indication of how well the models have performed. There are three main points to consider: the fit of the model to the PM dispersion profile, the fit of the model to the LOS dispersion profile, and the agreement of the PM and LOS dispersions.

In particular, we are interested in the shape of the model dispersion profile compared with the shapes of the data dispersion profiles. The only freedom we allow here is to change the distance or the (constant) *M/L*, these parameters have no power to change the shape of the model profile. Clusters for which the model and data profiles shapes are not consistent may indicate clusters for which the assumptions we introduced in Section 3.1 break down, as we will discuss further in Section 5.4.

For the majority of the clusters in our sample—NGC 104, NGC 288, NGC 1851, NGC 2808, NGC 5904, NGC 6266, NGC 6341, NGC 6397, NGC 6656, NGC 6715, NGC 6752, and NGC 7078—the agreement between PM dispersions, LOS dispersions, and model fits appears to be good, that is, everything is broadly consistent (albeit with no radial overlap between PM dispersions and LOS dispersions for NGC 5904). Where available for these clusters, the literature PM data also appears to be in good agreement with the rest of the data and the models, except for NGC 6397, where the literature PMs sit above both LOS data and model at the best-fit distance.
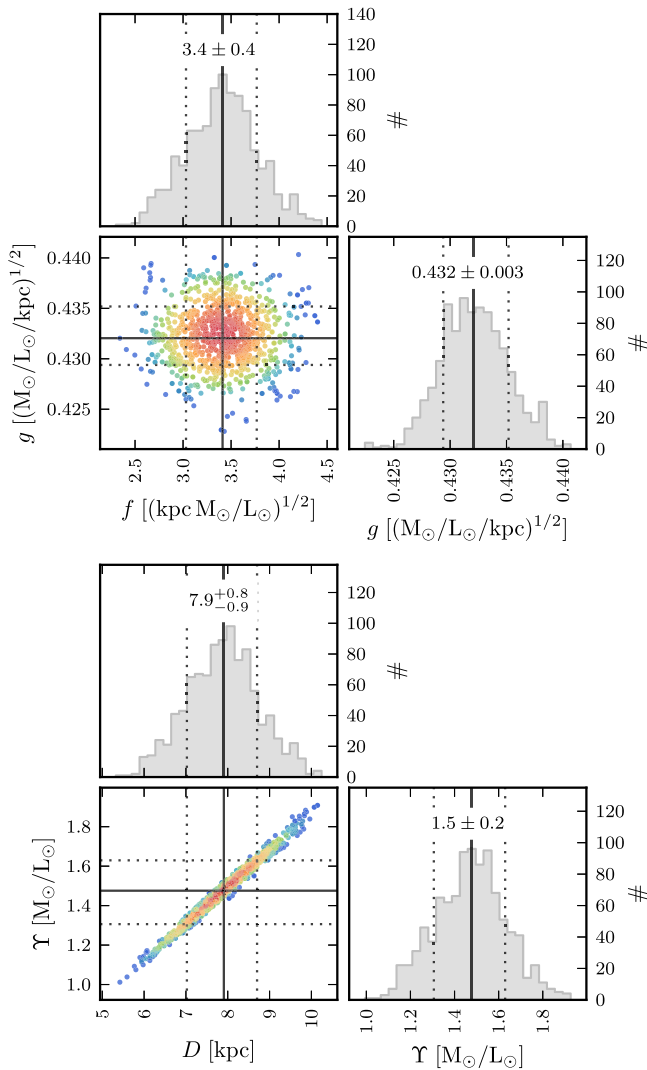
**Figure 4.** Final parameter distributions at the end of the MCMC run for NGC 5927. Histograms show the individual distributions; scatter plots show the combined distributions, with points colored by likelihood from high (red) to low (blue). The solid lines show the 50th percentiles of the distributions and the dotted lines show the 15.9th and 84.1th percentiles of the distributions. In the upper panels, we show parameters $f = \sqrt{D\Upsilon}$ and $g = \sqrt{\Upsilon/D}$. In the lower panels, we show distance $D$ and mass-to-light ratio $\Upsilon$ directly. Comparing the scatter plots, it is clear that $D$ and $\Upsilon$ are strongly correlated whereas $f$ and $g$ are uncorrelated, making it more effective to perform our parameter search in $(f, g)$ space.

For the three remaining clusters, the agreements between PM data, LOS data, and model are less convincing. For both NGC 5139 ($\omega$ Centauri) and NGC 6388, the shape of the model profile is a poor fit to both the PM and LOS profiles, implying that one or more of our assumptions were not valid for these clusters. Nevertheless, despite the poor models, the data profiles are consistent with each other so the distance estimation seems to have worked successfully and we include them in our subsequent analysis.

For NGC 5927, there is considerable scatter in the best-fitting models, though the models do seem to trace our PM data fairly well. Unfortunately, the restricted radial range of the LOS data leaves us with only three data points to use for that aspect of the fit. Although not ideal, this is enough for us to estimate a distance. Given the good agreement between PM data and

model here, we also include this cluster in our subsequent analysis.

Several of the cluster models in Figure 5 show central dips in their dispersion profiles. This is not unexpected. Spherical isotropic models with steep density profiles generically have this feature (e.g., Binney & Mamon 1982), and such dips are also seen in many dwarf elliptical galaxies (e.g., Geha et al. 2003). Although, if GCs do indeed host IMBHs at their centers then our models would be underestimates of the dispersion near the center and correctly accounting for the presence of an IMBH could make the dips disappear.

### 4.2. Mass Estimates

Our primary goal here is to estimate cluster distances. However, as a by-product of the distance estimation process, we estimate the *M/L* for each cluster. As the surface brightness profiles for the clusters are also known, we can use these *M/L*s to get the surface mass-density profiles for the clusters and, from there, total mass estimates for the clusters. The mass estimates are also shown in Table 2.

### 5. DISCUSSION

We wish to compare our dynamical distance and *M/L* estimates against previous photometric distances and population-synthesis *M/L* estimates to check for biases and systematic offsets. We also consider here the effects of the assumptions we made in Section 3.1.

### 5.1. Comparison with Photometric Distance Estimates

We have greatly expanded the number of dynamical distance estimates available, and all have been estimated using the same method. Both of these points will enable us to make a meaningful comparison to photometric distance estimates.

Here, we compare our dynamical-distance estimates with the (photometric) estimates from H96, which we include in Table 2. These estimates are suitable for this comparison as they were all derived in the same way (albeit from different data sets). The estimates were made using the mean magnitude of the observed horizontal branch $V_{HB}$ for each cluster. A simple calibration relation provides the absolute magnitude of the horizontal branch $M_{V,HB}$ given the cluster metallicity, from which the distance modulus $\mu = V_{HB} - M_{V,HB}$ and hence distance follow.

In Figure 6, we show the fractional difference between our distance estimates and the H96 distance estimates, defined as $(D_{our} - D_{Harris})/D_{Harris}$, as a function of our distance estimates. The dotted line marks a difference of zero. The solid line marks the mean of the fractional offsets and the shaded areas mark the $1\sigma$, $2\sigma$ and $3\sigma$ regions, where $\sigma$ is calculated as the error on the mean. The mean and $\sigma$ values are shown in the top right corner of the panel. The most distant cluster in the sample, by some margin, is NGC 6715 (M54); the rest of the clusters lie within 2 and 12 kpc from the Sun.

The unweighted mean of the offsets is consistent with zero at $-1.7 \pm 1.9\%$; this demonstrates that, on average, the dynamical and photometric estimates are in very good agreement over the whole sample. Although some clusters do show considerable disagreement between the dynamical and photometric estimates, this should be further investigated on a cluster-by-cluster basis. We see no evidence of a systematic offset biasing one method to over- or underpredict compared to the other.
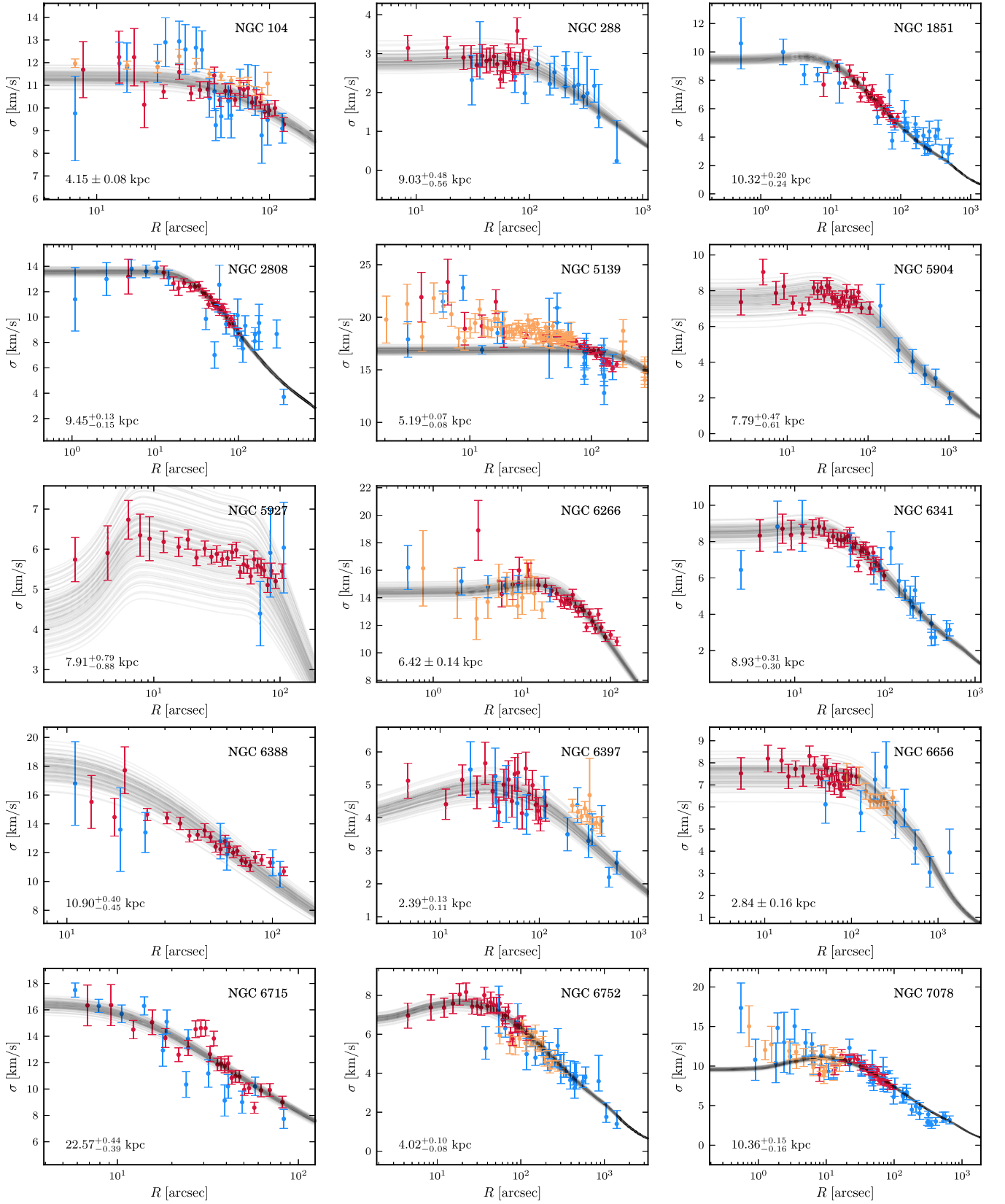
**Figure 5.** Velocity dispersion profiles and model fits for each of our clusters. Our PMs are shown in red, shifted to the best-fitting distance; the literature LOS velocities used for the fitting are shown in blue. 100 model draws from the final MCMC sample are shown as black lines. We give the distance estimate with uncertainties in the bottom left corner of each panel; note that the quoted uncertainties reflect the scatter in the fit due to random errors and do not account for further systematic errors due to incorrect modeling assumptions. Where available, we show literature PM dispersion profiles (also shifted to the best-fit distance) in orange; these are shown for comparison and were not used for the fits.

**Table 2**
Results: Distance and Mass-to-light Ratio Estimates

| Cluster | Other names | $N$ | $f$ $(\mathrm{kpc}\,M_\odot/L_\odot)^{0.5}$ | $g$ $(M_\odot/L_\odot/\mathrm{kpc})^{0.5}$ | $D$ (kpc) | $\Upsilon_V$ $(M_\odot/L_\odot)$ | $M_\mathrm{tot}$ $(10^5\,M_\odot)$ | $D_\mathrm{literature}$ (kpc) | $\Upsilon_{V,\mathrm{literature}}$ $(M_\odot/L_\odot)$ |
|---|---|---|---|---|---|---|---|---|---|
| (1) | (2) | (3) | (4) | (5) | (6) | (7) | (8) | (9) | (10) |
| NGC 104 | 47Tuc | 5631 | $2.41^{+0.05}_{-0.04}$ | $0.581^{+0.003}_{-0.004}$ | $4.15 \pm 0.08$ | $1.40 \pm 0.03$ | $5.57^{+0.33}_{-0.28}$ | 4.5 | 2.35 |
| NGC 288 | ⋯ | 713 | $4.44^{+0.24}_{-0.21}$ | $0.495^{+0.011}_{-0.012}$ | $9.03^{+0.48}_{-0.56}$ | $2.20^{+0.13}_{-0.10}$ | $0.79^{+0.13}_{-0.11}$ | 8.9 | 1.97 |
| NGC 1851 | ⋯ | 2810 | $3.95 \pm 0.08$ | $0.383 \pm 0.004$ | $10.32^{+0.20}_{-0.24}$ | $1.51 \pm 0.03$ | $1.78^{+0.10}_{-0.11}$ | 12.1 | 1.98 |
| NGC 2808 | ⋯ | 7867 | $3.84^{+0.05}_{-0.06}$ | $0.406 \pm 0.002$ | $9.45^{+0.13}_{-0.15}$ | $1.56 \pm 0.02$ | $5.91^{+0.22}_{-0.25}$ | 9.6 | 2.02 |
| NGC 5139 | $\omega$ Centauri | 16519 | $3.72 \pm 0.05$ | $0.716 \pm 0.003$ | $5.19^{+0.07}_{-0.08}$ | $2.66 \pm 0.04$ | $34.52^{+1.45}_{-1.43}$ | 5.2 | 1.87 |
| NGC 5904 | M5 | 2436 | $3.33^{+0.22}_{-0.25}$ | $0.429 \pm 0.004$ | $7.79^{+0.47}_{-0.61}$ | $1.43^{+0.09}_{-0.10}$ | $3.65 \pm 0.75$ | 7.5 | 1.96 |
| NGC 5927 | ⋯ | 5801 | $3.41^{+0.36}_{-0.38}$ | $0.432 \pm 0.003$ | $7.91^{+0.79}_{-0.88}$ | $1.48^{+0.15}_{-0.17}$ | $1.44^{+0.49}_{-0.43}$ | 7.7 | 2.93 |
| NGC 6266 | M62 | 7102 | $3.77^{+0.08}_{-0.07}$ | $0.587 \pm 0.004$ | $6.42 \pm 0.14$ | $2.22 \pm 0.04$ | $6.09^{+0.39}_{-0.33}$ | 6.8 | 1.95 |
| NGC 6341 | M92 | 2729 | $3.80^{+0.13}_{-0.11}$ | $0.426^{+0.004}_{-0.005}$ | $8.93^{+0.31}_{-0.30}$ | $1.62^{+0.06}_{-0.05}$ | $2.85^{+0.30}_{-0.25}$ | 8.3 | 1.93 |
| NGC 6388 | ⋯ | 6746 | $4.28^{+0.15}_{-0.17}$ | $0.392^{+0.003}_{-0.002}$ | $10.90^{+0.40}_{-0.45}$ | $1.68^{+0.06}_{-0.07}$ | $8.27^{+0.89}_{-0.95}$ | 9.9 | 2.55 |
| NGC 6397 | ⋯ | 517 | $2.31 \pm 0.09$ | $0.967^{+0.022}_{-0.023}$ | $2.39^{+0.13}_{-0.11}$ | $2.23^{+0.10}_{-0.09}$ | $0.70^{+0.09}_{-0.08}$ | 2.3 | 1.88 |
| NGC 6656 | M22 | 1924 | $2.31^{+0.13}_{-0.12}$ | $0.816 \pm 0.010$ | $2.84 \pm 0.16$ | $1.88^{+0.12}_{-0.11}$ | $2.49^{+0.44}_{-0.37}$ | 3.2 | 1.87 |
| NGC 6715 | M54 | 3790 | $6.61 \pm 0.10$ | $0.293^{+0.002}_{-0.003}$ | $22.57^{+0.44}_{-0.39}$ | $1.94 \pm 0.03$ | $11.83^{+0.62}_{-0.53}$ | 26.5 | 1.88 |
| NGC 6752 | ⋯ | 1860 | $2.93^{+0.06}_{-0.07}$ | $0.728 \pm 0.009$ | $4.02^{+0.10}_{-0.08}$ | $2.14^{+0.05}_{-0.06}$ | $1.82 \pm 0.12$ | 4.0 | 1.88 |
| NGC 7078 | M15 | 3107 | $3.92 \pm 0.05$ | $0.379 \pm 0.003$ | $10.36^{+0.15}_{-0.16}$ | $1.49 \pm 0.02$ | $4.95 \pm 0.19$ | 10.4 | 1.93 |

**Notes.** Columns: (1) cluster identification in the NGC catalog; (2) alternate name for cluster; (3) number of PM stars used for the distance estimation; (4) $f$ parameter used in fitting procedure; (5) $g$ parameter used in fitting procedure; (6) heliocentric distance estimate; (7) $V$-band mass-to-light ratio estimate; (8) total cluster mass estimate; (9) heliocentric distance from H96; (10) $V$-band mass-to-light ratio from McLaughlin & van der Marel (2005).

(This table is available in machine-readable form.)
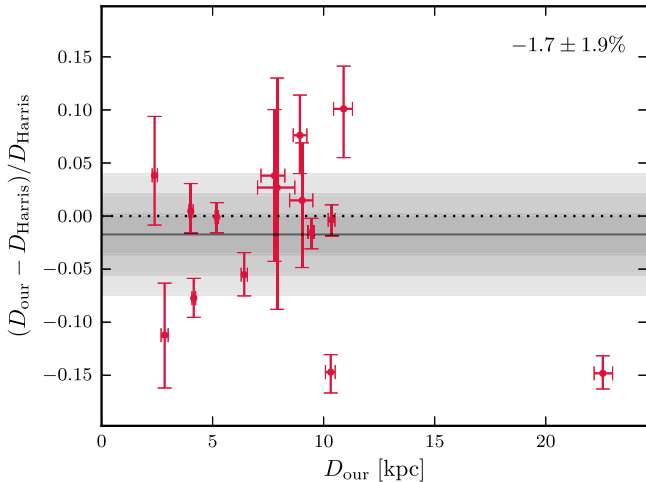


**Figure 6.** Comparison of our dynamical distance estimates with literature photometric distance estimates from H96. The red points show the fractional difference in distance as a function of our distance estimate for each of our clusters. The dotted line highlights zero, that is, perfect agreement between the two estimates. The solid line is the mean of the distance offsets and the shaded areas show the $1\sigma$, $2\sigma$ and $3\sigma$ regions, where $\sigma$ is the error on the mean. The mean and error are also shown in the top-right corner of the panel. Overall, the agreement between dynamical and literature distances is very good, suggesting that there are no significant biases in either estimation method.

Furthermore, neither the sign nor the magnitude of the offset correlate with cluster distance.

### 5.2. Comparison with Literature Dynamical Distance Estimates

For five clusters in our sample, dynamical distances have previously been estimated, so we now compare our estimates to these. As we shall see, overall our estimates are consistent with the earlier studies:

*NGC 104*. McLaughlin et al. (2006) estimated a dynamical distance of $4.0 \pm 0.35$ kpc, which is in good agreement with our estimate of $4.15 \pm 0.08$ kpc.

*NGC 5139 ($\omega$ Centauri)*. There have been three dynamical estimates for $\omega$ Centauri: $4.8 \pm 0.3$ kpc (van de Ven et al. 2006); $4.73 \pm 0.09$ kpc (van der Marel & Anderson 2010); and $4.59 \pm 0.08$ kpc (Watkins et al. 2013). All three studies attempted to account for the inner complexities of the cluster (rotation, anisotropy, flattening), which may explain why they are more similar to each other than to our estimate of $5.19^{+0.07}_{-0.08}$ kpc (which actually agrees better with the H96 photometric distance of 5.2 kpc).

*NGC 6266 (M62)*. McNamara & McKeever (2011) estimated a dynamical distance of $7.054 \pm 0.583$ kpc, which is consistent with our estimate of $6.42 \pm 0.14$ kpc at the $1\sigma$ level.

*NGC 6397*. Heyl et al. (2012) estimated a dynamical distance of $2.2^{+0.5}_{-0.7}$ kpc, which is consistent with our estimate of $2.39^{+0.13}_{-0.11}$ kpc.

*NGC 7078 (M15)*. There have been two previous dynamical distance estimates for this cluster: $10.3 \pm 0.4$ kpc (van den Bosch et al. 2006); and $9.98 \pm 0.47$ kpc (McNamara et al. 2004). Our estimate of $10.36^{+0.15}_{-0.16}$ kpc is in good agreement with both.

### 5.3. Comparison with Literature Mass-to-light Ratio Estimates

We also wish to compare our $M/L$ estimates with those already in the literature. For this comparison, we use the $M/L$s from McLaughlin & van der Marel (2005), which were estimated from population-synthesis models. They adopted cluster metallicities from H96 and a common age for all clusters of $13 \pm 2$ Gyr. Combining stellar population models for a given metallicity and age with an assumed initial mass function (IMF), they were able to estimate intrinsic colors and average $M/L$s. They provided six different estimates using different stellar-population (SP) codes and assuming different
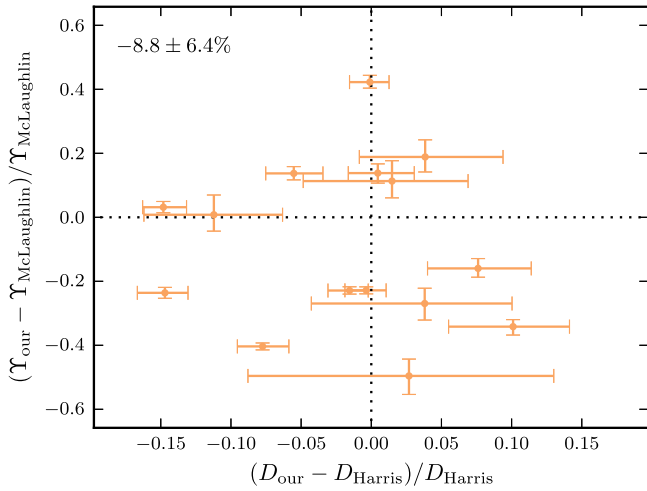
**Figure 7.** Comparison of dynamical distance and dynamical *M/L* estimates with literature photometric distances (H96) and population-synthesis *M/L* estimates (McLaughlin & van der Marel 2005). The orange points show the fractional offsets of our estimates from the literature values; the dotted lines highlight zero, or perfect agreement. The unweighted mean and error on the mean for the *M/L* offsets is shown in the top left corner of the panel. The corresponding value of the distance offsets was already show in Figure 6. The key point here is that the points are scattered across the whole figure, there is no correlation between the direction and magnitude of the distance and *M/L* offsets.

IMFs; to begin, we adopt the values calculated using the code presented in Bruzual & Charlot (2003) with a Chabrier (2003) disk IMF, as they did for their final analysis. These *M/L* estimates are included in Table 2.

As we did for the distances, we calculate the fractional difference between our *M/L* estimates and the McLaughlin & van der Marel (2005) *M/L* estimates, defined as $\left(\Upsilon_{\rm our} - \Upsilon_{\rm McLaughlin}\right)/\Upsilon_{\rm McLaughlin}$. In Figure 7, we show the fractional-distance differences and the fractional *M/L* differences. The dotted lines mark offsets of zero. The unweighted mean *M/L* offset and error on the mean are shown in the top-left corner of the panel. (The mean distance offset is already shown in Figure 6.)

The unweighted mean of the *M/L* offsets is consistent with zero at the $1.3\sigma$ level: $-8.8 \pm 6.4\%$. It is clear from the figure and from the means and errors that the fractional *M/L* differences are larger, in general, than the fractional distance differences. The *M/L* offsets are typically 20%–40%, while the distance offsets are typically within 10%. However, the scatter in the plot shows no correlation. The direction and magnitude of the distance offset is independent of the direction and magnitude of the *M/L* offset, thus indicating that our method is robust. Moreover, the good agreement of our *M/L* estimates with the McLaughlin & van der Marel (2005) estimates implies that a Chabrier (2003) disk IMF is consistent with our data for all clusters.

### 5.3.1. Initial Mass Functions

As previously mentioned, McLaughlin & van der Marel (2005) provided six different *M/L* estimates using different SP codes and different IMFs. We now compare our dynamical *M/L* estimates with each of these population-synthesis estimates. Once again, we calculate the fractional offset of our measurements from the population-synthesis estimates and

**Table 3**
Consistency of Different Population-synthesis *M/L* Estimates

| Model<br>(1) | Code<br>(2) | IMF<br>(3) | $\Delta\Upsilon$<br>(4) |
|---|---|---|---|
| 1 | BC | Chabrier (disk) | $-8.8 \pm 6.4$ |
| 2 | BC | Salpeter | $-45.7 \pm 3.9$ |
| 3 | PEGASE | Chabrier (disk) | $-17.9 \pm 5.8$ |
| 4 | PEGASE | Salpeter | $-50.6 \pm 3.6$ |
| 5 | PEGASE | Chabrier (GC) | $-8.6 \pm 6.6$ |
| 6 | PEGASE | Kroupa | $-15.0 \pm 6.1$ |

**Notes.** Columns: (1) population-synthesis model; (2) SP code used to compute model (BC—Bruzual & Charlot 2003, PEGASE—Fioc & Rocca-Volmerange 1997 v2.0); (3) IMF used for model (sources: Chabrier 2003; Salpeter 1955; Kroupa et al. 1993); (4) fractional offset of the population-synthesis *M/L*s from our dynamical *M/L*s. The population-synthesis *M/L* estimates were all taken from McLaughlin & van der Marel (2005).

calculate the mean and the standard error on the mean. The models are summarized and *M/L* offsets are reported in Table 3.

Irrespective of the SP code used to perform the modeling, we see that our dynamical *M/L* estimates and the population-synthesis estimates using a Salpeter (1955) IMF (models 2 and 4) are significantly different. The offsets are at the level of $12\sigma$ using the Bruzual & Charlot (2003) code and $14\sigma$ using the PEGASE code (Fioc & Rocca-Volmerange 1997). We strongly rule out a Salpeter (1955) IMF for Galactic GCs.

The remaining models used a Chabrier (2003) disk IMF (models 1 and 3), a Chabrier (2003) GC IMF (model 5) or a Kroupa et al. (1993) IMF (model 6). All are consistent with our *M/L* estimates, given the random errors inherent in our analysis and uncertainties due to the modeling and details of the SP codes.

### 5.3.2. Mass-to-light Ratio Variation with Metallicity

Strader et al. (2011) estimated dynamical *V*-band *M/L*s for a set of 200 GCs in M31 and found that their *M/L* estimates tend to decrease with increasing cluster metallicity. This behavior directly opposes predictions from population-synthesis models that *M/L*s should increase with increasing cluster metallicity. So let us now consider how our *M/L* estimates vary with cluster metallicity, which values we take from H96.

In Figure 8, we show our dynamical *M/L* estimates as a function of cluster metallicity (blue points). For comparison, we show the Strader et al. (2011) M31 cluster data (black points) and the McLaughlin & van der Marel (2005) *M/L* estimates for our clusters (green points, again using metallicities from H96). The distribution of our *M/L* estimates is consistent with the Strader et al. (2011) estimates across the full range of metallicities and exhibits the same decrease in *M/L* that Strader et al. (2011) saw at the metal-rich end of the M31 cluster distribution. Our estimates are also consistent with the McLaughlin & van der Marel (2005) population-synthesis estimates for the metal-poor clusters (as we would expect given the generally good agreement overall discussed in the previous section) but deviate for the most metal-rich clusters.

Strader et al. (2011) argued that this behavior is not caused by dynamical evolution inside the cluster and instead favor a modification to population-synthesis models (in the form of a shallower mass function for metal-rich GCs) to bring the dynamical estimates and population-synthesis estimates into better agreement. However, Shanahan & Gieles (2015) showed
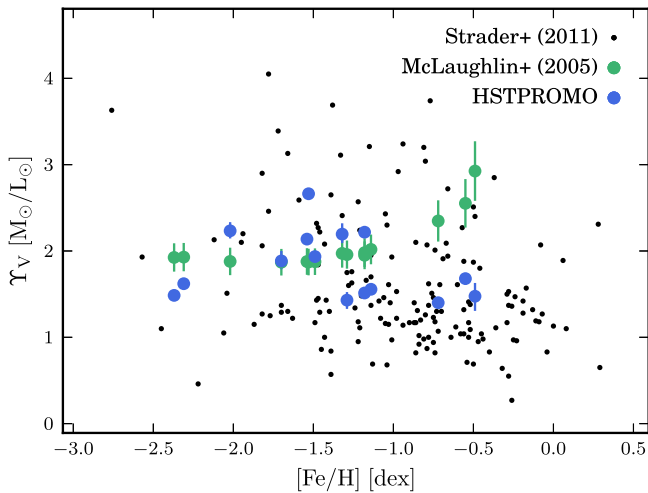
**Figure 8.** *M/L* estimates as a function of metallicity. The blue points show our dynamical *M/L* estimates, with metallicities taken from H96. For comparison, the black points show the dynamical *M/L* estimates for a sample of M31 GCs from Strader et al. (2011), which tend to decrease with increasing metallicity; the green points show the population-synthesis *M/L* estimates from McLaughlin & van der Marel (2005) for our clusters, which tend to increase with increasing metallicity. Our estimates are consistent with the Strader et al. (2011) M31 clusters over the full range of metallicities but deviate from the population-synthesis estimates at high metallicities.

that this phenomenon may indeed be dynamical in origin and attribute it to mass segregation in the cluster. It is beyond the scope of this work to further investigate the origin of this phenomenon, however, the full PM catalogs are well-suited to studying mass segregation in clusters and this is a topic we plan to address in future papers.

## 5.4. Effect of Modeling Assumptions

For the modeling part of this analysis, we assumed that our clusters are spherical, isotropic, non-rotating, and have a constant *M/L*. For 12 of our 15 clusters, the models were generally good fits to both the PM and LOS data. This suggests that our assumptions were reasonable for these clusters; we cannot be certain, though it seems convenient that the effect of a number of incorrect assumptions would cancel out so well. However, let us briefly consider what we do know about these clusters and the quality of the assumptions we have made.

### 5.4.1. Shape

The assumption of sphericity implies that quantities of interest vary only with radius and not with position angle, so we can consider one-dimensional radial profiles. We demonstrated in Paper 2 that many of our catalogs contain sufficient data to study two-dimensional spatial variations in velocity dispersion, however, most LOS velocity data sets are too small to obtain two-dimensional dispersion maps. (Indeed, many LOS velocity data sets are so small that obtaining one-dimensional profiles can be a challenge.) Furthermore, we require surface brightness profiles for our modeling here, and these are only available as one-dimensional profiles for most clusters. Deriving two-dimensional surface-brightness profiles is beyond the scope of this paper. Reassuringly, the two-dimensional dispersion maps we showed in Paper 2 did not reveal a high degree of flattening in our clusters.

White & Shawl (1987) provide ellipticities for 14 of the well-fit clusters (only NGC 288 is missing from their list): the values range from 0.01 for NGC 6266 to 0.14 for NGC 5904 and NGC 6656. In fact, there are four clusters with ellipticities of 0.1 or higher. We might expect the assumption of sphericity to break down for these moderately flattened clusters, however, we see no correlation between distance offset and ellipticity. This supports the notion that ignoring ellipticity does not systematically bias the distance estimates.

### 5.4.2. Anisotropy

We showed in Paper 2 that the clusters in our sample are very close to isotropic at their centers. Some clusters do show some radial anisotropy with increasing radius, but the effect is very mild. In most cases, the LOS velocity data extends beyond our PM data; however, even if we extrapolate the anisotropy profiles from Paper 2 to cover the range of the LOS velocity data, the anisotropy is still small. Paper 2 measured projected anisotropy and not intrinsic anisotropy, which is key when considering LOS data alongside our PM data. However, Section 2.7.3 of van der Marel & Anderson (2010) shows that projected and intrinsic anisotropy are directly linked, so our expectation of isotropy or at most mild anisotropy, still holds.

Furthermore, we average out the impact of anisotropy by combining both radial and tangential PMs together when calculating our PM dispersion profiles. For steep density profiles, anisotropy will tend to increase one component of motion while decreasing another component of motion by an approximately equal factor so that their mean remains approximately the same. Although this behavior can break down for flatter density profiles, such as those we observe for GCs (e.g., Cappellari 2015); we performed tests to verify that this is not the case for our clusters. In general, averaging the PMs together does tend to wash out any anisotropy.

Finally, the good agreement between our distances and the Harris photometric estimates suggests that the assumption of isotropy is reasonable.

### 5.4.3. Rotation

We assume that the clusters are not rotating—this is a necessary assumption because our PM catalogs contain only relative motions and not absolute motions, thus washing out any rotation signatures. As we discussed in detail in Paper 2, the lack of any rotation signature does not affect the dispersions that we measure. We also know that rotation will generally increase with radius, and as our PM measurements are confined to the central regions, we do not expect significant signal from rotation in our PM data.

For the LOS data sets, rotation has the potential to be more of a concern. The key point to consider here, again, is that we expect little to no rotation at the center where the LOS data overlaps with our PM data. The good agreement between LOS data and models in the outer regions for most clusters would suggest that rotation is not significant in most cases. However, recall that there were three clusters for which we restricted the range of the LOS data to be only the region that overlapped with our PM data due to poor model fits. For these clusters, it is possible that rotation may become significant in the outer regions and should be included for an improved model fit outside of the range of our PM data.

### 5.4.4. Mass-to-light Ratio

We assume that mass follows light in clusters, so the mass-density profile is simply a scaled version of the luminosity-density profile; the scale factor is, of course, the *M/L*. As they evolve, clusters move toward a state of energy equipartition, the effect of which is that massive (bright) stars tend to move more slowly than the low-mass (faint) stars. As a result, the more-massive (brighter) stars sink toward the center of the cluster and therefore have a more concentrated density profile than the less-massive (fainter) stars. This is mass segregation. Owing to the different luminosity-density and mass-density profiles created by this mass segregation (Kruijssen 2008), we might expect that the cluster *M/L* will change with radius.

In principle, our dynamical models could allow the *M/L* to change as a function of radius; however, for our analysis, we assume that the *M/L* is constant through the cluster. The *M/L* at a fixed radius will affect both PM and LOS measurements equally, so a radially-varying *M/L* is only an issue in cases for which the radial coverage of the PM data and LOS data are different. Once again, the good agreement between model and data, even in cases where the radial coverage of the different data types are not consistent, indicates that the assumption of constant (or nearly constant) *M/L* through the clusters is reasonable. It is possible that the clusters for which we restricted the range of the LOS data to have an *M/L* that varies with radius, but the effect is mitigated by considering only the LOS data that overlaps with our PM data.

Further support for the assumption of a constant *M/L* comes from van de Ven et al. (2006) who showed that the *M/L* of $\omega$ Centauri (NGC 5139) is constant over a wide range of radii. Though it is worth noting that $\omega$ Centauri may harbor an intermediate-mass black hole (IMBH) at its center—results are conflicting (Noyola et al. 2010; van der Marel & Anderson 2010). IMBHs are believed to limit the amount of mass segregation in a cluster because they act as a source of energy at the cluster center (Baumgardt et al. 2005; Gill et al. 2008); so if $\omega$ Centauri does host an IMBH, we would expect little mass segregation and a fairly flat *M/L*.

IMBHs are not the only mechanism by which mass segregation can be quenched; any source of energy at the center will achieve the same effect. A significant population of binaries or a segregated population of stellar-mass black holes at the center of the cluster can also inhibit mass segregation throughout the rest of the cluster (e.g., Mackey et al. 2008). So there are a number of factors that determine the degree of mass segregation and, hence *M/L* variation in a cluster.

The degree of segregation within clusters has been studied for individual clusters (e.g., Pasquato et al. 2009; Beccari et al. 2010) and for large samples of clusters (e.g., Goldsbury et al. 2013). Fourteen of our fifteen clusters are in the Goldsbury et al. (2013) sample; most show some mass segregation but it is relatively mild. A notable exception is NGC 6388, which shows considerable mass segregation. This may explain why the shape of the Jeans models deviated from the shape of the velocity dispersion profiles, though, recall that the velocity profiles themselves did show good agreement, despite the poor shape of the model.

## 6. CONCLUSIONS

We have determined dynamical distance and *M/L* estimates for 15 Galactic GCs. To do this, we combined PM dispersion profiles determined from the *HST* PM catalogs described in Paper 1 with LOS dispersion profiles compiled from literature sources. To these dispersion profiles, we then fitted dynamical models from which we were able to estimate distances and *M/Ls*. For the majority of our clusters, no PM data was previously available, so this is the first dynamical distance and *M/L* study performed.

Although the distance estimates themselves are a useful product of this work, the driving force behind this study was to check for consistency between dynamical distance estimates and photometric distance estimates. To this end, in Section 5.1, we compared our dynamical distances with photometric distance estimates from H96. A key point in this comparison is the homogeneity of the data analyses that we compared; the data for each cluster are necessarily different, as each cluster is unique; however, both here and in H96, the data was treated in a uniform way. This helps to eliminate some possible sources of contention and allows for a more robust comparison.

We showed that the dynamical and photometric distance estimates were consistent with each other within their uncertainties. The mean fractional difference between the two types of estimate was just $-1.9 \pm 1.7\%$. This indicates that there are no significant biases in either method that may cause one to under- or overestimate the cluster distances with respect to the other. This also provides an important validation of the stellar evolution theory that underlies photometric distance estimates. Furthermore, neither the sign nor the magnitude of the fractional distance offset correlate with cluster distance.

A side product of this analysis was the estimation of dynamical *M/L* values for each cluster. We compared these against the population-synthesis *M/L* values determined in McLaughlin & van der Marel (2005). Pleasingly, the values agreed within $1.3\sigma$ (the mean fractional *M/L* offset was $-8.8 \pm 6.4\%$), and we detected no correlation between our *M/L* offsets from literature values and our distance offsets from literature values. This provides a strong indication that our methods were reliable and our results are robust.

Furthermore, we compared our dynamical *M/L* estimates with a set of population-synthesis *M/L* estimates (also from McLaughlin & van der Marel 2005) which assumed different IMFs: we ruled out a Salpeter (1955) IMF at high significance, but were unable to distinguish between a Chabrier (2003) disk IMF, a Chabrier (2003) GC IMF and a Kroupa et al. (1993) IMF. We also found that our *M/L* estimates tend to decrease with increasing metallicity; this behavior directly opposes predictions from SP models, but supports a similar trend observed in a sample of 200 M31 clusters by Strader et al. (2011).

Paper 1 provided catalogs for 22 Galactic GCs; however, we were only able to use 15 clusters for this analysis. Of the clusters we did not include here, two clusters—NGC 6362 and NGC 7099—have LOS literature data, but we found that our PM catalogs (after cleaning) were too small to perform a reliable analysis. For these, it is possible that a more tailored cleaning algorithm would yield more usable stars than the one-size-fits-all cleaning we performed here—this is beyond the scope of this paper but would be an interesting topic for future work.

For the remaining five clusters—NGC 362, NGC 6441, NGC 6535, NGC 6624, and NGC 6681—there were no LOS data available in the literature that were sufficient for our purposes here. This illuminates an important shift in dynamical cluster studies. Although LOS measurements and PM measurements are both lacking for clusters, until now, lack of PM data
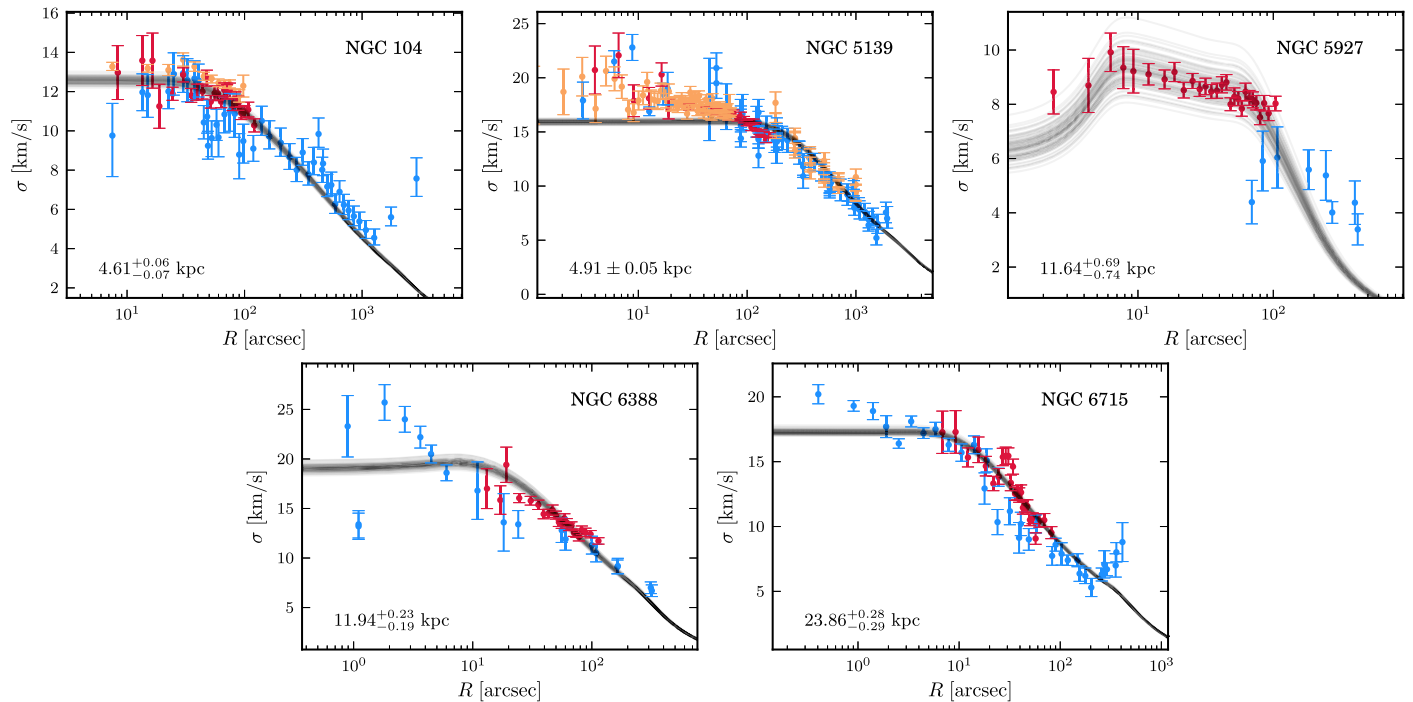
**Figure 9.** Full fits for restricted clusters.

has been the biggest drawback. However, we are now in a situation where we have some clusters with LOS data but no PM data, and some clusters with PM data but no LOS data. These five clusters would be prime targets for observing campaigns in the near future in order to obtain larger LOS data sets that could augment the kinematic information provided by our PM catalogs.

## APPENDIX A
## RESTRICTING LITERATURE DATA

During preliminary analysis of our clusters, we found that five had several inconsistencies between our PM data, literature LOS data, and the model fit. Figure 9 shows the initial results for these five clusters. As for Figure 5, red points show our PM data and blue points show literature LOS data; the black line show the models fits to the red and blue points. Orange points show literature PM data, where available, for comparison only and were not used for fitting. Let us consider each in turn.

*NGC 104*. Here, the model is a reasonable fit to the LOS data where it overlaps with our PM data, but underestimates the LOS data in the outer regions. This is likely due to the break down of our assumptions in the outer regions of the cluster (see discussion in Section 5.4). The anomalous two outermost data-points are attributable to evaporation (Lane et al. 2010); their inclusion or exclusion does not significantly alter the fit.

*NGC 5139*. Here, the models do a very poor job at fitting both the LOS dispersions and the PM dispersions. However, as we mentioned in Section 3.1, $\omega$ Centauri is well-known to be anisotropic, rotating and highly flattened, so it is not surprising that even the best model does not fit the data well. We expect that anisotropy, rotation and flattening will all be more significant and intermediate and large radii, that is, in regions beyond the extent of our PM data.

*NGC 5927*. The peculiar shape of the surface brightness profile for this cluster (see Figure 3) gives rise to a peculiar shape for the model dispersion profiles, though the models do seem to trace our PM data fairly well. However, the models fail to accurately reproduce the shape of the LOS dispersion profile outside of the range of our PM data.

*NGC 6388*. Here, the model is a very poor fit to the data in the central regions of the cluster. This is due to the considerable controversy regarding the shape of the dispersion profile near the center. Studies of individual radial velocities (Lanzoni et al. 2013; Lardo et al. 2015) argue that the dispersion profile stays flat at the center, while studies using Integral Field Spectroscopy (IFS) measure a dispersion that rises steeply toward the center Lützgendorf et al. (2011) (as would be expected if the cluster harbours an IMBH at its center). The PM profile used for the present study does not extend far enough into the center to comment on either of these claims.[11]

---

[11] This will require more careful cleaning of the data and more detailed modeling, and will be the topic of a future paper.

**Table 4**
Compilation of Literature Dispersion Profiles

| Cluster | $R$ | $\Delta R$ | $\sigma$ | $\Delta\sigma^+$ | $\Delta\sigma^-$ | Type | Source | |
| --- | --- | --- | --- | --- | --- | --- | --- | --- |
| | (arcsec) | | | (km s$^{-1}$) | | | | |
| (1) | (2) | (3) | (4) | (5) | (6) | (7) | (8) | |
| NGC 104 | 13.525 | 4.593 | 11.967 | 0.939 | 0.939 | LOS | Gebhardt et al. | (1995) |
| | 24.967 | 2.510 | 12.898 | 1.079 | 1.079 | LOS | Gebhardt et al. | (1995) |
| | 32.605 | 2.217 | 12.582 | 1.096 | 1.096 | LOS | Gebhardt et al. | (1995) |
| | 40.639 | 2.227 | 12.564 | 0.839 | 0.839 | LOS | Gebhardt et al. | (1995) |
| | 48.045 | 2.293 | 10.726 | 0.842 | 0.842 | LOS | Gebhardt et al. | (1995) |
| | 57.730 | 4.777 | 10.309 | 0.796 | 0.796 | LOS | Gebhardt et al. | (1995) |
| | 140.017 | 47.826 | 10.512 | 0.744 | 0.744 | LOS | Gebhardt et al. | (1995) |
| | 457.745 | 157.683 | 8.015 | 0.643 | 0.643 | LOS | Gebhardt et al. | (1995) |
| | 7.500 | 0.000 | 9.760 | 1.640 | 2.090 | LOS | McLaughlin et al. | (2006) |
| | 15.000 | 0.000 | 11.820 | 1.050 | 1.130 | LOS | McLaughlin et al. | (2006) |

**Notes.** Columns: (1) cluster ID; (2)–(3) radius and uncertainty; (4)–(6) dispersion and uncertainty; (7) data type; (8) data source. All PM dispersions have been converted from mas yr$^{-1}$ to km s$^{-1}$ using the distance from H96. These distances are also provided in Table 2.

(This table is available in its entirety in machine-readable form.)

*NGC 6715.* For this cluster, the model fails to trace the central rise of the literature LOS dispersion profile or the sharp upturn in the outer regions of the cluster. However, the model is broadly consistent with the LOS data in the region of overlap with our PM data.

In an attempt to improve the fits, we restrict the range of the literature LOS data used for the fitting of these clusters to be only those data points that overlap with our PMs. That is, if our PM dispersion profile has an innermost bin at $R_{\rm in} \pm \Delta R_{\rm in}$ and an outermost bin at $R_{\rm out} \pm \Delta R_{\rm out}$, we restrict the range of the literature data to be $R_{\rm in} - \Delta R_{\rm in} \leqslant R \leqslant R_{\rm out} + \Delta R_{\rm out}$.

For some of these clusters, the inconsistencies are only apparent outside of the range of our PM data, so by restricting the data in this way, we can eliminate problem areas. For others, the fits seem generally poor, but by restricting the range of the LOS data to the region of overlap with our PM data, we hope to at least mitigate any problems outside of the region of our data. As discussed further in Section 4.1, the fits are greatly improved for NGC 104 and NGC 6715, but still show some inconsistencies for NGC 5139, NGC 5927, and NGC 6388.

It is important to note that restricting the LOS data as we have described here is not the same as fudging the result. In essence, our goal is simply to align the LOS and PM profiles in the radial range where they overlap. Employing dynamical models, as we have done here, allows us to also use the data in the radial range where they do not overlap. This is only improvement if the models are to be trusted and provide a good fit. If they do not fit the data at large or small radii, then this approach actually makes the results worse than when only using the data in the radial overlap region.

## APPENDIX B
## COMPILATION OF LITERATURE DATA

Table 4 provides the compilation of literature velocity dispersion profiles used for this paper, as described in Section 2.3 and summarized in Table 1. This table contains profiles for all clusters together. The columns list: the name of the cluster; the radial coordinate (and uncertainty, where available); the velocity dispersion, with uncertainty, of the stars in the bin; the type of data (PM or LOS); and the data source.

REFERENCES

Astropy Collaboration, Robitaille, T. P., Tollerud, E. J., et al. 2013, A&A, 558, A33
Baumgardt, H., Makino, J., & Hut, P. 2005, ApJ, 620, 238
Beccari, G., Pasquato, M., De Marchi, G., et al. 2010, ApJ, 713, 194
Bellazzini, M., Ibata, R. A., Chapman, S. C., et al. 2008, AJ, 136, 1147
Bellazzini, M., Ibata, R., Ferraro, F. R., & Testa, V. 2003, A&A, 405, 577
Bellini, A., Anderson, J., van der Marel, R. P., et al. 2014, ApJ, 797, 115
Bianchini, P., Varri, A. L., Bertin, G., & Zocchi, A. 2013, ApJ, 772, 67
Binney, J., & Mamon, G. A. 1982, MNRAS, 200, 361
Bruzual, G., & Charlot, S. 2003, MNRAS, 344, 1000
Cappellari, M. 2002, MNRAS, 333, 400
Cappellari, M. 2008, MNRAS, 390, 71
Cappellari, M. 2015, arXiv:1504.05533
Carretta, E., Bragaglia, A., Gratton, R. G., et al. 2006, A&A, 450, 523
Carretta, E., Bragaglia, A., Gratton, R. G., et al. 2010, A&A, 520, A95
Carretta, E., Bragaglia, A., Gratton, R. G., Lucatello, S., & Momany, Y. 2007, A&A, 464, 927
Carretta, E., Gratton, R. G., Clementini, G., & Fusi Pecci, F. 2000, ApJ, 533, 215
Carretta, E., Lucatello, S., Gratton, R. G., Bragaglia, A., & D'Orazi, V. 2011, A&A, 533, A69
Catelan, M., Pritzl, B. J., & Smith, H. A. 2004, ApJS, 154, 633
Chaboyer, B. 1995, ApJL, 444, L9
Chabrier, G. 2003, PASP, 115, 763
Cowan, J. J., Sneden, C., Burles, S., et al. 2002, ApJ, 572, 861
Del Principe, M., Piersimoni, A. M., Storm, J., et al. 2006, ApJ, 652, 362
den Brok, M., van de Ven, G., van den Bosch, R., & Watkins, L. 2014, MNRAS, 438, 487
Drukier, G. A., Cohn, H. N., Lugger, P. M., et al. 2007, AJ, 133, 1041
Drukier, G. A., Slavin, S. D., Cohn, H. N., et al. 1998, AJ, 115, 708
Emsellem, E., Cappellari, M., Krajnović, D., et al. 2011, MNRAS, 414, 888
Feldmeier, A., Lützgendorf, N., Neumayer, N., et al. 2013, A&A, 554, A63
Fioc, M., & Rocca-Volmerange, B. 1997, A&A, 326, 950
Foreman-Mackey, D., Hogg, D. W., Lang, D., & Goodman, J. 2013, PASP, 125, 306
Gebhardt, K., Pryor, C., Williams, T. B., & Hesser, J. E. 1995, AJ, 110, 1699
Geha, M., Guhathakurta, P., & van der Marel, R. P. 2003, AJ, 126, 1794
Gill, M., Trenti, M., Miller, M. C., et al. 2008, ApJ, 686, 303
Goldsbury, R., Heyl, J., & Richer, H. 2013, ApJ, 778, 57
Goodman, J., & Weare, J. 2010, Commun. Appl. Math. Comput. Sci., 5, 65
Hansen, B. M. S., Brewer, J., Fahlman, G. G., et al. 2002, ApJL, 574, L155
Harris, W. E. 1996, AJ, 112, 1487
Heyl, J. S., Richer, H., Anderson, J., et al. 2012, ApJ, 761, 51
Ibata, R., Bellazzini, M., Chapman, S. C., et al. 2009, ApJL, 699, L169
Kamann, S., Wisotzki, L., Roth, M. M., et al. 2014, A&A, 566, A58
Kimmig, B., Seth, A., Ivans, I. I., et al. 2015, AJ, 149, 53
Krauss, L. M., & Chaboyer, B. 2003, Sci, 299, 65
Kroupa, P., Tout, C. A., & Gilmore, G. 1993, MNRAS, 262, 545
Kruijssen, J. M. D. 2008, A&A, 486, L21

Küpper, A. H. W., Balbinot, E., Bonaca, A., et al. 2015, ApJ, 803, 80
Lane, R. R., Kiss, L. L., Lewis, G. F., et al. 2009, MNRAS, 400, 917
Lane, R. R., Kiss, L. L., Lewis, G. F., et al. 2010, MNRAS, 401, 2521
Lanzoni, B., Mucciarelli, A., Origlia, L., et al. 2013, ApJ, 769, 107
Lapenna, E., Origlia, L., Mucciarelli, A., et al. 2015, ApJ, 798, 23
Lardo, C., Pancino, E., Bellazzini, M., et al. 2015, A&A, 573, A115
Lovisi, L., Mucciarelli, A., Lanzoni, B., et al. 2012, ApJ, 754, 91
Lützgendorf, N., Kissler-Patig, M., Noyola, E., et al. 2011, A&A, 533, A36
Lützgendorf, N., Kissler-Patig, M., Gebhardt, K., et al. 2012, A&A, 542, A129
Lützgendorf, N., Kissler-Patig, M., Gebhardt, K., et al. 2013, A&A, 552, A49
Mackey, A. D., & Gilmore, G. F. 2004, MNRAS, 355, 504
Mackey, A. D., Wilkinson, M. I., Davies, M. B., & Gilmore, G. F. 2008, MNRAS, 386, 65
Martin, N. F., Ibata, R. A., Bellazzini, M., et al. 2004, MNRAS, 348, 12
McLachlan, G. J., & Peel, D. 2000, Finite Mixture Models (New York: Wiley)
McLaughlin, D. E., Anderson, J., Meylan, G., et al. 2006, ApJS, 166, 249
McLaughlin, D. E., & Meylan, G. 2003, in ASP Conf. Ser. 296, New Horizons in Globular Cluster Astronomy, ed. G. Piotto et al. (San Francisco, CA: ASP), 153
McLaughlin, D. E., & van der Marel, R. P. 2005, ApJS, 161, 304
McNamara, B. J., Harrison, T. E., & Anderson, J. 2003, ApJ, 595, 187
McNamara, B. J., Harrison, T. E., & Baumgardt, H. 2004, ApJ, 602, 264
McNamara, B. J., Harrison, T. E., Baumgardt, H., & Khalaj, P. 2012, ApJ, 745, 175
McNamara, B. J., & McKeever, J. 2011, AJ, 142, 163
Mészáros, S., Dupree, A. K., & Szalai, T. 2009, AJ, 137, 4282
Meylan, G., & Mayor, M. 1991, A&A, 250, 113
Niederste-Ostholt, M., Belokurov, V., Evans, N. W., et al. 2010, MNRAS, 408, L66
Noyola, E., Gebhardt, K., Kissler-Patig, M., et al. 2010, ApJL, 719, L60
Pasquato, M., Trenti, M., De Marchi, G., et al. 2009, ApJ, 699, 1511
Salpeter, E. E. 1955, ApJ, 121, 161
Scarpa, R., & Falomo, R. 2010, A&A, 523, A43
Scarpa, R., Marconi, G., Carraro, G., Falomo, R., & Villanova, S. 2011, A&A, 525, A148
Scarpa, R., Marconi, G., Gilmozzi, R., & Carraro, G. 2007, Msngr, 128, 41
Schlafly, E. F., & Finkbeiner, D. P. 2011, ApJ, 737, 103
Seth, A. C., van den Bosch, R., Mieske, S., et al. 2014, Natur, 513, 398
Shanahan, R. L., & Gieles, M. 2015, MNRAS, 448, L94
Simmerer, J., Feltzing, S., & Primas, F. 2013, A&A, 556, A58
Sollima, A., Bellazzini, M., & Lee, J.-W. 2012, ApJ, 755, 156
Sollima, A., Bellazzini, M., Smart, R. L., et al. 2009, MNRAS, 396, 2183
Sollima, A., & Nipoti, C. 2010, MNRAS, 401, 131
Strader, J., Caldwell, N., & Seth, A. C. 2011, AJ, 142, 8
Trager, S. C., King, I. R., & Djorgovski, S. 1995, AJ, 109, 218
Trenti, M., & van der Marel, R. 2013, MNRAS, 435, 3272
Vandenberg, D. A., Bolte, M., & Stetson, P. B. 1996, ARA&A, 34, 461
van den Bosch, R., de Zeeuw, T., Gebhardt, K., Noyola, E., & van de Ven, G. 2006, ApJ, 641, 852
van den Bosch, R. C. E., van de Ven, G., Verolme, E. K., Cappellari, M., & de Zeeuw, P. T. 2008, MNRAS, 385, 647
van der Marel, R. P., & Anderson, J. 2010, ApJ, 710, 1063
van de Ven, G., van den Bosch, R. C. E., Verolme, E. K., & de Zeeuw, P. T. 2006, A&A, 445, 513
Verde, L., Jimenez, R., & Feeney, S. 2013, PDU, 2, 65
Watkins, L. L., Evans, N. W., Belokurov, V., et al. 2009, MNRAS, 398, 1757
Watkins, L. L., van de Ven, G., den Brok, M., & van den Bosch, R. C. E. 2013, MNRAS, 436, 2598
Watkins, L. L., van der Marel, R. P., Bellini, A., & Anderson, J. 2015, ApJ, 803, 29
White, R. E., & Shawl, S. J. 1987, ApJ, 317, 246
Zloczewski, K., Kaluzny, J., Rozyczka, M., Krzeminski, W., & Mazur, B. 2012, AcA, 62, 357